JOURNAL OF CATALYSIS 96, 481–490 (1985)

The Formation of Filamentous Carbon on Iron and Nickel Catalysts

III. Morphology

E. BOELLAARD, P. K. DE BOKX, A. J. H. M. KOCK, AND J. W. GEUS

Department of Inorganic Chemistry, State University of Utrecht, Croesestraat 77A, 3522 AD Utrecht, The Netherlands

Received May 31, 1984; revised February 18, 1985

The microstructure of primary carbon filaments formed on supported iron and nickel catalysts has been investigated using transmission electron microscopy, dark-field imaging, and (selected-area) electron diffraction. It has been established that the filaments consist of cone-shaped graphite layers, stacked with their *c*-axes in a direction normal to the metal–carbon interface. A growth mechanism is proposed involving the excretion of cone-shaped graphite layers. To explain the constancy of the filament diameter, slippage of these layers over one another is invoked. Edge dislocations are brought about by differences in the rate of carbon excretion.

INTRODUCTION

In Parts I and II (*1, 2*) we provided evidence for the involvement of metastable carbide intermediates in carbon filament growth on iron and nickel catalysts. It was established that high carbide contents are a prerequisite for the nucleation of carbon. In this paper our aim is to elucidate the structure of the filamentous carbon as well as to reveal the way in which the carbide precursor influences the structural order of the carbon.

The degree of this order in filamentous carbon strongly depends on the physical conditions at the point of deposition (*3*). A clear distinction should be made between the structure of primary filamentous carbon and of pyrolytic filamentous carbon, the latter being formed by thermal cracking of hydrocarbons at temperatures above 870 K (*4*). Primary filamentous carbon can be characterized by a filament diameter equal to that of the metal particle at the tip, whereas pyrolytic filamentous carbon is recognized by diameters greatly exceeding the diameter of the original metal particle (Fig. 1). These different filament morphologies result from different growth processes. Evidence has been given that the pyrolytic thickening process is preceded by the formation of thin primary filaments (*5*).

X-Ray examinations on the well-ordered pyrolytic carbon have revealed that the *c*-axis of graphite is oriented roughly perpendicular to the fiber axis with a maximum deviation of 30° (*6*). Oberlin *et al.* (*7*), using a lattice-imaging technique, provided evidence that the pyrolytic carbon layers near the more electron-transparent coaxial tubes are perfectly parallel, whereas the relative misorientation of carbon layers in the external part of the fiber ranges from 20 to 30°.

Primary filamentous carbon deposits were thoroughly studied by Audier *et al.* (*8, 9*). Metal–carbon composites were obtained by disproportionation of CO using mixtures of CO and CO_2 at atmospheric pressure and temperatures between 720 and 920 K. They focused on the determination of the crystallographic relations between the metal particles and the carbon filaments as a function of the crystalline structure of the metal. In most cases hollow filaments were investigated, well-defined metal faces being exposed at the inner side of the car-

0021-9517/85 $3.00

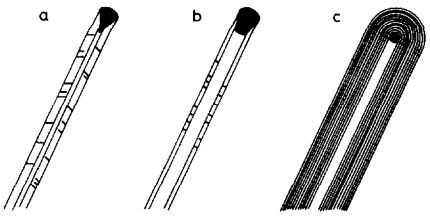

FIG. 1. Different types of filamentous carbon; (a) primary carbon filament with a metal particle at the tip and a narrow electron-transparent canal, (b) primary carbon filament with a metal particle at the tip and a wide canal (tube), (c) pyrolytic filamentous carbon. The metal (carbide) particle of the original primary filament is trapped within the pyrolytic carbon.

bon tube. It was established that graphite layers were oriented almost parallel with the tube axis. No carbide or oxide formation was detected after filament growth in the case of bcc alloys (FeCo). The crystallographic [100] axis of the alloy particle was found to coincide with the filament axis. They observed the metal particles at the tip to be cone-shaped, the basal faces always being spanned by (100) planes. The absence of carbon deposits on (100) faces (*10*) provides an explanation for the occurrence of hollow primary filaments. For alloys of fcc structure (FeCo, FeNi) Audier *et al.* (*8, 9*) provided evidence that the [110] axis of the conical particles coincides with the carbon tube axis, while the metal–gas interface consists of (111) planes. Finally, they proved that carburization of Fe resulted in the formation of a cone-shaped Fe_7Ce_3 particle (Eckstrom-Adcock carbide), having an orthorhombic structure (*11*). The metal particle was composed of two microcrystals with a common (110) face, displaying two (010) faces at the metal–gas interface. Robertson (*12*) also established that in fibrous specimens of carbon, deposited by methane decomposition over iron and nickel at 923 and 1023 K, the carbon crystallite basal planes (the (0001) planes) are preferentially oriented parallel to the fiber axis. An arced electron diffraction pattern was observed, indicative of either a degree of misfit between successive graphite layers or of the occurrence of a number of different orientations within the selected area, used for obtaining the diffraction pattern.

It was the intent of this investigation to discriminate between the two explanations above for the occurrence of the arced diffraction pattern. In the opinion of the present authors a sound knowledge of graphitic order is indispensable in understanding the high mechanical strength of the fibers responsible for the destruction of the support structure of the catalyst (*13*).

EXPERIMENTAL

Specimen preparation. Nickel catalysts (50 wt% metal loading) were prepared by precipitation of Ni(II) ions from an aqueous solution onto a suspended silica support by means of homogeneous urea decomposition at 363 K (*14*).

Iron catalysts (20 wt%) were prepared according to the procedure described by Boudart *et al.* (*15*) using basic magnesium carbonate (Riedel-de Haën, p.a.) as a support precursor.

Carburization was usually performed in a flow of CO/H_2 or CH_3OH/N_2 (0.8 $cm^3\ s^{-1}$) using an atmospheric flow reactor; after reaction samples were quenched in an inert gas flow to room temperature and subsequently passivated in an oxygen/nitrogen mixture. Samples of carburized catalysts were pretreated by ultrasonic dispersion in ethanol. A small drop of the suspension was deposited onto a holey carbon film supported by a copper grid.

Microscopy and diffraction. Both a Jeol 200 C (200 kV) and a Philips EM 420 (100 kV) electron microscope were used in transmission electron microscopy and selected-area electron diffraction experiments. High-resolution dark-field images were produced by tilting the incident beam until coincidence of a selected diffracted beam with the optic axis of the microscope was attained. This was realized by means of the incorporated deflection coils, mounted above the specimen. By tilting the beam in

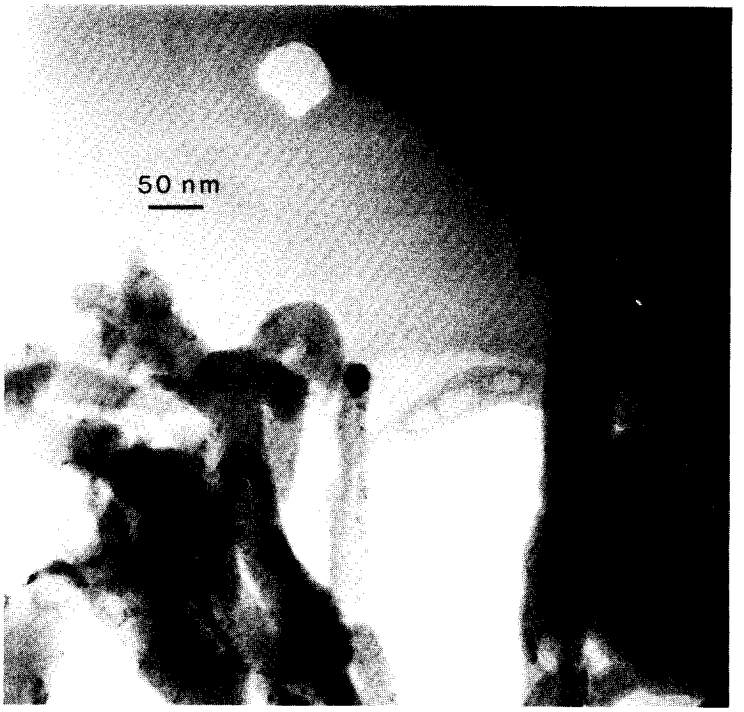

FIG. 2. Electron micrograph (TEM) displaying excessive filamentous carbon deposition on a 50 wt% Ni catalyst after prolonged carburization at 850 K (CO/H_2 ratio: 0.5).

this way the spherical aberration which reduces the resolution was kept to a minimum.

The relative rotation between the transmission image and the corresponding diffraction pattern was established for all operating conditions. This calibration was carried out by employing a double-exposure technique in which the diffraction pattern and the transmission image of a crystal of molybdenum trioxide are recorded successively.

The specimen was mounted on a sample holder which could be rotated along two independent axes. Diffraction patterns were measured by means of a microdensitometer (Jenoptik MD 100) and calibration was performed with the accurately known pattern of a polycrystalline gold film.

RESULTS

Figure 2 illustrates excessive filamentous carbon deposition formed during prolonged methanation experiments on a nickel catalyst at 850 K. The CO/H_2 ratio was kept at 0.5. The filaments are characterized by relatively electron-transparent canals along their axes and an inhomogeneously streaked texture. With increasing diameter of the filaments the texture is more pronounced. Metal particles at the tip of these primary filaments in general exhibit a cone-shaped appearance. Figure 3 shows a particular filament, diameter 70 nm, striking by its straightness. Such a filament is especially suited for investigation of its carbon microstructure, as it contains only one well-defined direction of its axis. Selected-area electron diffraction performed on this filament gives the pattern depicted in Fig. 4. On indexing the pattern the most pronounced diffraction intensity was shown to be consistent with the (0002) reflection of graphite. From the figure it is apparent that two distinct orientations of the graphite layers are present. To localize these orienta-

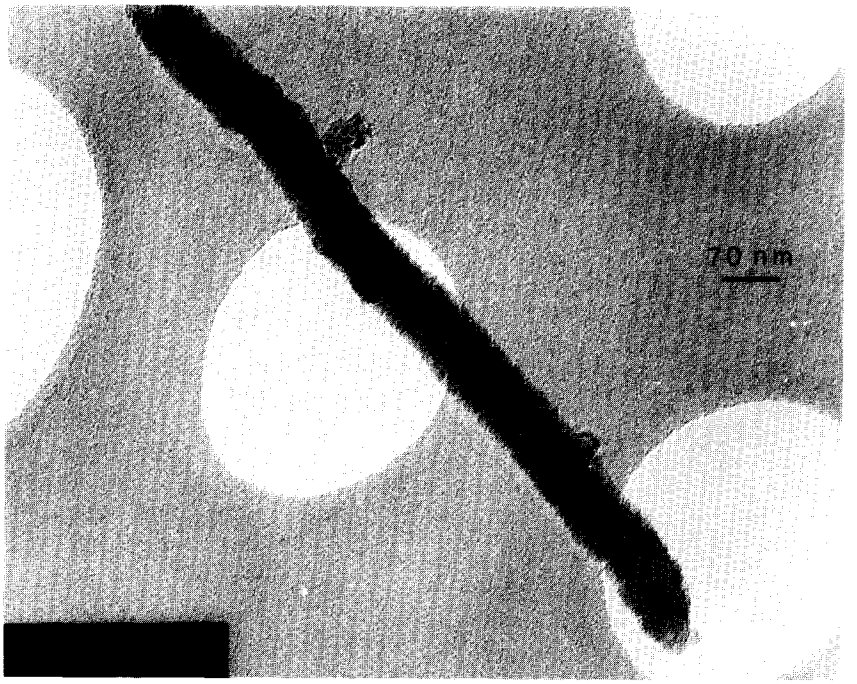

FIG. 3. Carbon filament of remarkable straightness (TEM); experimental conditions as in Fig. 2.

tions in the filament the incident electron beam was tilted in the plane spanned by the optic axis of the microscope and the (0002) diffraction beam until coincidence of the latter beam with the optic axis was attained. In this way (0002) reflections of known orientation were used as the imaging radiation in obtaining the dark-field images of Figs. 5 and 6. These images demonstrate that the two different orientations are localized on opposite sides of the fiber axis. The angle between the two orientations of the graphite *c*-axes varies over a wide range. It was established that the direction of the streaked texture mentioned above corresponds to the *c*-direction of graphite.

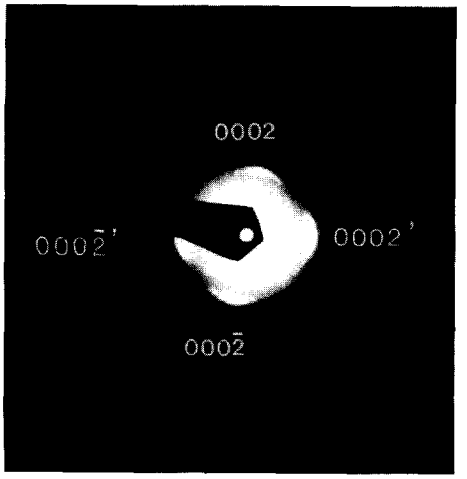

FIG. 4. Selected-area electron diffraction pattern of the carbon filament displayed in Fig. 3.

In earlier reports it was suggested that this texture was brought about by metal clusters (*13, 16*). Superposition of the diffraction intensity originating from the Ni $(11\bar{1})$ reflection and that from the graphite $(10\bar{1}1)$ reflection calls for the use of a well-defined imaging diffraction ring in obtaining dark-field electron micrographs. It is now clear from the dark-field experiments that the majority of the streaks in bright-field are due to diffraction contrast originating from mutually parallel graphite layers. It should be noted that the planes at the ends of the filaments (V-shaped in cross section) are oriented perpendicular to the *c*-direction, i.e., they are closest packed graphite lay-

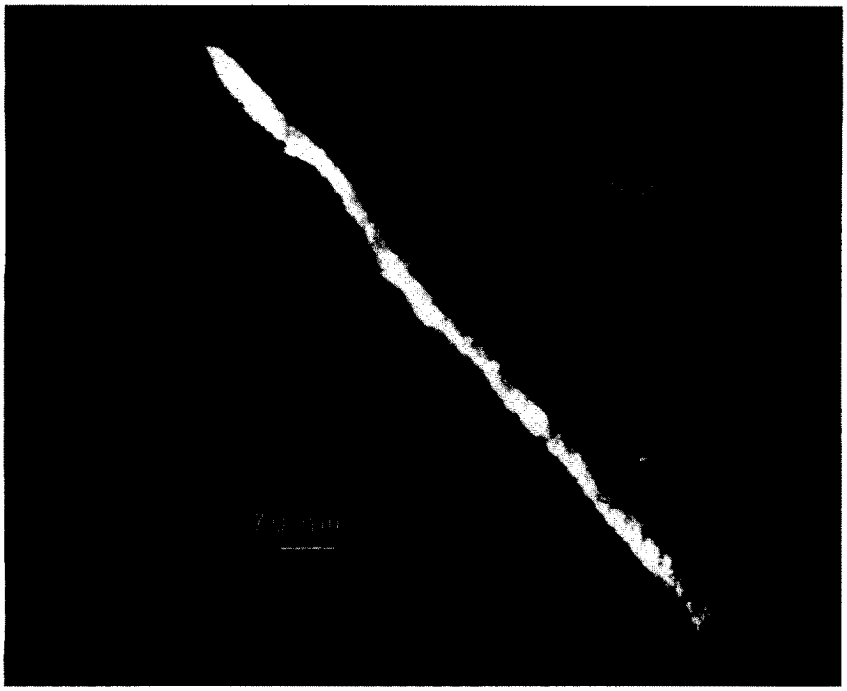

FIG. 5. Dark-field image obtained employing the (0002) electron beam.

FIG. 6. Dark-field image obtained employing the (0002′) electron beam.

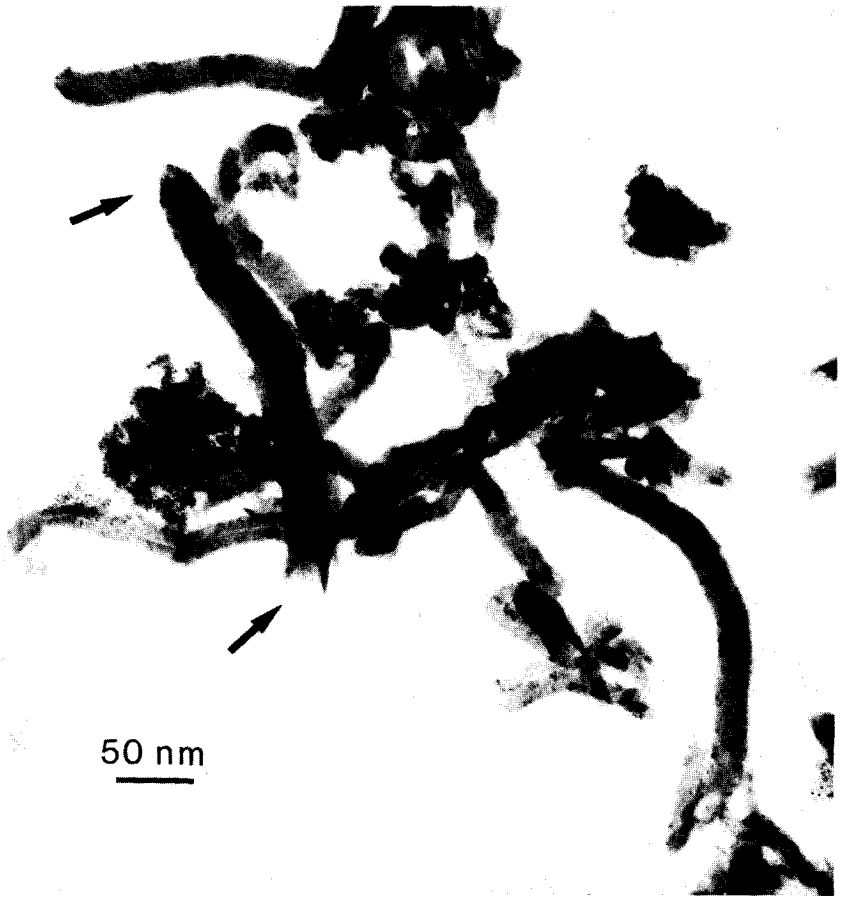

FIG. 7. Electron micrograph illustrating cleavage of filaments along graphitic basal planes; a number of cleavage planes is indicated by means of arrows.

ers. The frequent occurrence of these closest packed layers at the ends of the filaments, as well as the existence of both V-shaped filament ends and their counterparts (Fig. 7) indicate that these planes are cleavage planes. Also experiments were performed in which the filament was rotated about its axis. The electron diffraction pattern during rotation over 100° remained exactly the same as represented in Fig. 4, suggesting a high symmetry along the filament axis.

In Fig. 8 the electron diffraction pattern of a nickel particle is shown. When the cone axis was brought to coincidence with the rotation axis of the sample holder, the cone top angle of the metal (carbide) particle did not change on rotation. This proves that the metal (carbide) cone is aligned in the plane perpendicular to the incident beam. The metal cone axis was found to coincide with the $[11\bar{2}]$ direction of the nickel crystallite, in contrast to the general rule for fcc alloys proposed by Audier *et al.* (*9*).

Also in the case of iron catalysts generally two distinct orientations of graphite layers were observed in the primary filaments (Fig. 9). In preliminary experiments using methane, carbon monoxide, or methanol as carburizing agents and magnesia, alumina, or graphite as support materials this carbon microstructure was observed in all samples. These results indicate that the

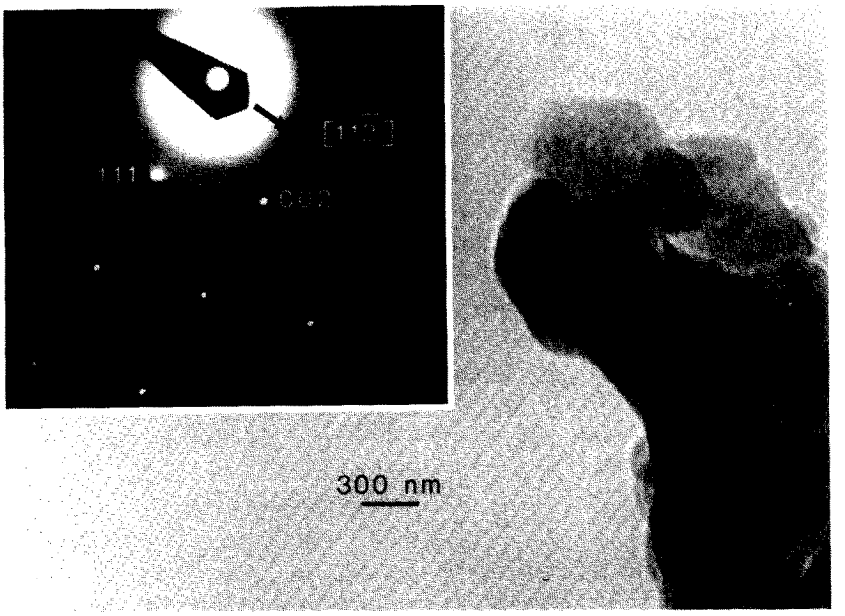

FIG. 8. Electron micrograph of a nickel particle with inserted selected-area electron diffraction pattern (corrected for image rotation). The axis of the nickel cone is shown to be aligned along the [11$\bar{2}$] direction. The projection direction is [1$\bar{1}$0].

FIG. 9. Electron micrograph of a 20 wt% Fe/MgO catalyst after carburization with a 7 vol% CH_3OH/N_2 mixture at 800 K. Insert: a typical dark-field image illustrating the carbon texture.

carbon structure is determined by the growth mechanism rather than by the nature of the metal, support, or carburizing agent. It should be noted that with carburized iron catalysts also carbon morphologies are observed which differ from the filaments described above. A fraction of these filaments do not display the regular mirror symmetry along the filament axis. The iron particles at the tip of these filaments often have an irregular shape. No diffraction patterns indicative of Eckstrom-Adcock carbide were observed.

DISCUSSION

Our observations indicate that filamentous carbon exhibits a very distinct carbon order. This structure seems to be determined by the shape of the metal particle at the tip of the filament. The way these metal particles acquire the cone shape is not clear. In a previous paper, however, we provided evidence that in the early stages of growth part of the nickel becomes inaccessible to magnetic measurements, i.e., it ends up in small clusters (*2*). One could imagine that this nickel is lost during the erosion process leading to cone-shaped metal crystallites.

Carbon often displays turbostratic character, i.e., closest packed layers can be mutually displaced in directions normal to the *c*-axis of graphite (*17*). This is manifested in the appearance of only ($hk\bar{h} + k0$) and (000 $2l$) reflections in X-ray diffraction experiments. The lubricity of graphite can be attributed to the easy slippage of the closest packed layers over one another. On the other hand, carbon structures of considerable mechanical strength are characterized by lack of this freedom of movement. High-tensile fibers owe their physical qualities to a tree-like carbon configuration (*18*). The graphite layers are cylindrically and coaxially arranged. This order is induced by a drastic recrystallization of carbon at temperatures up to 3170 K (*19*).

The carbon microstructure in the filaments which we investigated can be represented by a fishbone-like arrangement of the graphite basal planes. It should be realized that electron diffraction intensity originates from lattice planes approximately parallel to the incident electron beam (due to the small electron wavelength). Hence the fishbone arrangement of graphite layers is rigorously proved only for the cross section of the filament normal to the incident beam. The rotation experiments, however, demonstrate an almost cylindrical symmetry, displaying the graphite layers to be conically ordered, indicative of a cone-shaped metal particle as was observed earlier by Audier *et al.* (*9*). The mechanical strength of these conically ordered filaments is responsible for the destruction of the catalyst support structure. However, the strength is lower than that of the high-tensile fibers mentioned above, witnessed by the frequent occurrence of cleavage planes at the ends of the filaments.

In the above we presented a description of the structure of primary carbon filaments following directly and unequivocally from our experiments. As we concluded from the generality of the observed structure that a specific growth mechanism may be held responsible for the observed morphology, we now turn to an admittedly rather speculative proposal for the growth mechanism. Any suggested mechanism explaining primary filament growth should be consistent with the following observations: (i) carbon is transported through the bulk of the metal matrix (*20, 22*) by means of simultaneous formation and decomposition of a substoichiometric carbide (*1, 2*), (ii) the diameter of the filament remains constant over very large distances, and (iii) the order between successive graphite layers within the filament is not homogeneous. Along the filament axis, areas with perfect parallelism between successive graphite layers are alternated with areas of poor order.

A priori a number of mechanisms could be proposed. A possible presupposition is that complete cones made up by graphite layers are excreted consecutively from the

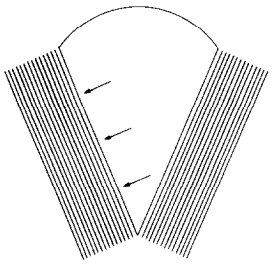

FIG. 10. Cross section of conical graphite layers excreted from the metal particle in a direction perpendicular to the metal–carbon interface.

metal particle without slippages of the already formed graphite layers over one another (Fig. 10). When carbon atoms are excreted in a direction perpendicular to the metal–carbon interface, and no slippage is allowed, the perimeter of earlier formed cones is forced to increase, resulting in bursting of the cones. Such a mechanism is not consistent with requisite (ii). Starting with the same assumption, but now allowing for slippage, a situation would result as represented in Fig. 11. Graphite layers successively excreted are pushing the metal particle in the direction of the filament axis and the diameter of the filament does not change. However, in this case dark-field images would not exhibit a streaked texture, but the diffraction due to perfectly parallel graphitic carbon layers would be exhibited homogeneously. Actually, excretion of carbon in a direction perpendicular to the metal–carbon interface, followed by slippage of graphite layers over one another, is indistinguishable from excretion in a direction parallel to the filament axis. However, when carbon atoms are preferentially excreted in a particular direction characteristic of the metal involved, a specific cone angle would be expected. Our results contradict the existence of a characteristic cone angle. As excretion of complete cones is not consistent with the observed texture, we propose a mechanism in which the rate of carbon excretion is not uniform over the entire metal cone surface. This seems plausible realizing that carbon transport through the metal particle is known to be the rate-determining step in filamentous growth (*20, 22*). Consequently, sites at the metal–carbon interface near the metal–gas interface (i.e., the cone circumference) suffer less from lack of carbon supply than do sites at larger distances from the metal–gas interface. If the flux of carbon atoms is dependent on the position on the metal–carbon interface, different numbers of graphite layers are produced in a given period of time. Hence, due to the local insertion of cone fragments, edge dislocations are introduced. Previously excreted graphite layers are forced to adjust to the presence of edge dislocations as depicted in Fig. 12. Consequently, local graphitic order

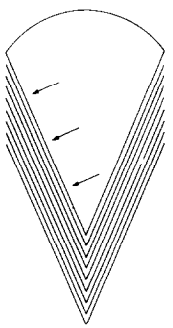

FIG. 11. Cross section of conical graphite layers excreted in a direction perpendicular to the metal–carbon interface, followed by slippage of the graphitic cones over one another.

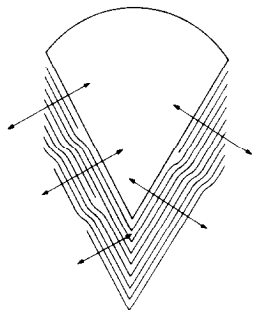

FIG. 12. Cross section of conical graphite layers excreted in a direction perpendicular to the metal–carbon interface, followed by excretion of the graphitic cones over one another; the rate of carbon excretion is not uniform over the metal–carbon interface, so edge dislocations are introduced. The length of the arrows indicates the local degree of order.

will be disturbed. As a result the graphitic order observed in dark-field micrographs is restricted to small domains unaffected by the above edge dislocations. In Fig. 12 arrows indicate domains of well-ordered graphite. A mechanism involving excretion of cone-shaped graphite layers, accompanied by differences in the rate of carbon excretion, is consistent with requisites (i), (ii), and (iii).

CONCLUSIONS

(i) Carbon filaments essentially consist of cone-shaped graphite layers.

(ii) Excreted graphite layers are parallel with the metal–carbon interface.

(iii) A tentative explanation for the origin of the observed graphite stacking involves: (1) a slippage of excreted graphite layers during growth to maintain the cone coherence, and (2) differences in the rate of carbon supply as a function of the position on the metal–carbon interface, bringing about the edge dislocations, which are responsible for the streaked texture in the dark-field images.

ACKNOWLEDGMENTS

The authors are indebted to Dr. E. G. M. Kuijpers for supplying carburized Ni samples. The investigations were supported by the VEG Gasinstituut n.v. and by the Netherlands Foundation for Chemical Research (SON) with financial aid from the Netherlands Organization for the Advancement of Pure Research (ZWO).

REFERENCES

1. de Bokx, P. K., Kock, A. J. H. M., Boellaard, E., Klop, W., and Geus, J. W., *J. Catal.* **96,** 454 (1985).
2. Kock, A. J. H. M., de Bokx, P. K., Boellaard, E., Klop, W., and Geus, J. W., *J. Catal.* **96,** 468 (1985).
3. Robertson, S. D., *Carbon* **10,** 221 (1972).
4. Rostrup-Nielsen, J. R., and Tøttrup, P. B., *in* "Proc. Symp. Sci. Catal. Its Appl. Ind. 1979", p. 379. Fert. (Plann. Dev.), India Ltd. Sindri, India
5. Koyama, T., and Endo, M., *Jpn. J. Appl. Phys.* **13,** 1175 (1974).
6. Hillert, M., and Lange, N., *Z. Kristallogr.* **111,** 24 (1958).
7. Oberlin, A., Endo, M., and Koyama, T., *J. Cryst. Growth* **32,** 335 (1976).
8. Audier, M., Coulon, M., and Oberlin, A., *Carbon* **18,** 73 (1980).
9. Audier, M., Oberlin, A., and Coulon, M., *J. Cryst. Growth* **55,** 549 (1981).
10. Kehrer, V. J., Jr., and Leidheiser, H., Jr., *J. Phys. Chem.* **58,** 550 (1954).
11. Audier, M., Bowen, P., and Jones, W., *J. Cryst. Growth* **63,** 125 (1983).
12. Robertson, S. D., *Carbon* **8,** 365 (1970).
13. Rostrup-Nielsen, J. R., *in* "Catalysis, Science and Technology" (J. R. Anderson and M. Boudart, Eds.), Vol. 5, p. 73. Springer, Berlin, 1984.
14. Hermans, L. A. M., and Geus, J. W., *in* "Studies of Surface Science and Catalysis," No. 3 (B. Delmon, P. Grange, P. Jacobs, G. Poncelet, Eds.), p. 113. Elsevier, Amsterdam, 1979.
15. Boudart, M., Delbouille, A., Dumesic, J. A., Khammouma, S., and Topsøe, H., *J. Catal.* **37,** 486 (1975).
16. Kuijpers, E. G. M., Tjepkema, R. B., and Geus, J. W., *J. Mol. Catal.* **25,** 241 (1984).
17. Klug, H. P., and Alexander, L. E., *in* "X-Ray Diffraction Procedures," p. 667. Wiley, New York, 1974.
18. Stewart, M., *J. Aust. Ceram. Soc.* **9,** 56 (1973).
19. Burghard, W., Umeno, M., Wiech, G., and Zahorowski, W., *J. Phys. C.* **16,** 4243 (1983).
20. Baker, R. T. K., Yates, D. J. C., and Dumesic, J. A., *in* "Coke Formation on Metal Surfaces" (L. F. Albright and R. T. K. Baker, Eds.), ACS Symposium Series 202, p. 1. Amer. Chem. Soc., Washington, D.C., 1982.
21. Trimm, D. L., *Catal. Rev.-Sci. Eng.* **16,** 155 (1977).
22. Rostrup-Nielsen, J. R., and Trimm, D. L., *J. Catal.* **48,** 155 (1977).